Hindawi
Shock and Vibration
Volume 2021, Article ID 3751146, 19 pages
https://doi.org/10.1155/2021/3751146

Research Article

Mechanism of Coal Burst and Prevention Practice in Deep Asymmetric Isolated Coal Pillar: A Case Study from YaoQiao Coal Mine

Chengchun Xue,[1] **Anye Cao**,[1] **Wenhao Guo**,[1] **Songwei Wang**,[1] **Yaoqi Liu**,[1] **and Zhiping Shen**[2]

[1]*School of Mines, China University of Mining and Technology, Xuzhou, Jiangsu 221116, China*
[2]*Datun Energy Company Limited, Xuzhou 221600, Jiangsu, China*

Correspondence should be addressed to Anye Cao; caoanye@163.com

Received 19 July 2021; Revised 16 August 2021; Accepted 20 December 2021; Published 29 December 2021

Academic Editor: Pengfei Wang

Coal pillar bursts continue to be a severe dynamic hazard. Understanding its mechanism is of paramount importance and crucial in preventing and controlling its occurrence. The extreme roadway deformations from the asymmetric isolated coal pillars in the central mining district of YaoQiao Coal Mine have responded with frequent intense tremors, with risky isolated coal pillar bursts. The theoretical analysis, numerical simulation, and field measurements were done to research the impact of spatial overburden structure and stress distribution characteristics on the isolated coal pillar area, aiming to reveal the mechanism of coal pillar burst leading to the practice of prevention and control in the asymmetric isolated coal pillar area. The study shows that the overburden structure of the asymmetric is an asymmetric "T" structure in the strike-profile, and the stress in the coal pillar is mostly asymmetric "saddle-shaped" distribution, with the peak stress in the east side of the coal pillar, and the coal pillar is a "high stress serrated isolated coal pillar." Numerical simulation results showed that the support pressure in the isolated coal pillar area on the strike profile was asymmetrically "saddle-shaped" distribution. The peak vertical stress in the coal pillar area continued to rise and gradually shifted to the mining district's deep part. As a result, the response of the roadway sides to the dynamic load disturbance was more pronounced. They developed a coal burst prevention and control program of deep-hole blasting in the roof of asymmetrical isolated coal pillar roof and unloading pressure from coal seam borehole. Monitored data confirmed that the stress concentration was influential in the roadway's surrounding rock in the asymmetric isolated coal pillar area, circumventing coal pillar burst accidents. The research outcomes reference the prevention and control of coal bursts at isolated working faces of coal pillars under similar conditions.

1. Introduction

Coal bursts, a dynamic geological hazard in underground coal mining, are characterized by coal and rock masses' sudden and violent failure with a significant energy release. They posed a severe threat to the production and safety of underground coal mining or surface buildings and, in some cases, resulted in injury and loss of life [1, 2]. In recent years, with the increase in the depth and intensity of coal mining in China, mining conditions have deteriorated dramatically, and the frequency of coal burst accidents has a rising trend [3]. The occurrence of coal burst was closely related to the degree of stress concentration in the coal and rock layer and the overburden structure in the working face [4, 5]. With the gradual hollowing out of the working face on both sides of the mining district roadway, the protection coal pillar area gradually formed an isolated structure. With hollowing on both sides, the static stress load concentration of the roadway surrounding the rock system in the isolated coal pillar area is high. When it was affected by thick and hard rock layer breaking and working face mining disturbance, the isolated coal pillar area was affected by the superposition

of concentrated load. The higher was the possibility of inducing coal pillar bursts [6]. For example, On March 27, 2014, a coal burst occurred during the return roadway excavation period in the 21032 mining district: six workers died and thirteen workers were injured [7]. On August 15, 2014, a coal burst occurred in 35000 mining district, where a 300 m long mining road was damaged, two workers were killed [8]. It was common in mine production to form isolated protection coal pillars after extensive hollowing on both sides of the mining district. Therefore, it was essential to study the mechanism of coal bursts in isolated protection coal pillar areas to protect the pedestrian and ventilation and transportation tasks in the mining district roadway.

Chen et al. [9] studied the overlying rock movement and stress distribution over the equivalent mining height method over isolated coal pillars. Jia et al. [10] analyzed the overburden damage pattern and coal pillar deformation characteristics during mining the isolated working face under thick and hard critical seam conditions based on similar material simulation tests. Hao et al. [11] theoretically analyzed the rock movement characteristics and stress distribution pattern of the isolated working face, and the theoretical criterion for safe mining of the isolated working face was proposed. Fuxing et al. [12] analyzed the dynamic change process of the roof structure in irregular mining areas on both sides during work face retrieval. They presented the calculation formula of coal body support pressure and destabilization analysis method for an isolated working face. Li et al. [13] studied dynamic stress evolution in the isolated protective pillar during the long wall panel analysis using PFC2D. The computational model of abutment pressure was established by theoretically analyzing the stress transfer mechanism of the two types of roof structure, and the calculation method for abutment stress was proposed [14]. Reed et al. [15] studied the mechanical characteristics of the coal pillar system and proposed the interaction mechanism between coal pillars and overburden. Hamid [16] studied that, through the methods of field observation, geological monitoring, and numerical simulation, the horizontal stress accumulation in the coal pillar-topside-bottom plate was quantitatively analyzed. It was concluded that the horizontal stress in the high-stress coal pillar and the surrounding rock would cause impact and trigger the violent destabilization of the coal pillar.

Many scholars researched the stability of isolated coal pillars from the overburden structure and stress distribution characteristics of the isolated working face (or isolated coal pillar) and made many research findings. Still, the research on coal burst induced by the instability of asymmetric isolated coal pillars (size asymmetry of coal pillar and size asymmetry of goaf on both sides) is rare. Moreover, coal burst hazards are subject to different coal pillars and various impact hazards, which are difficult to prevent and control. Thus, the coal burst accident induced by the overall instability of asymmetric isolated coal pillars is an emotional disaster problem that needs addressing in coal mine safety production.

YaoQiao Coal Mine's central mining district protecting coal pillar, on both sides of an extensive range of mining void and size irregularities, formed an asymmetric isolated coal pillar area. On August 25, 2016, a coal burst event (Figure 1, red star area), magnitude up to 1.9 on the Richter scale, resulting in the return roadway over a 60 m range, of the return roadway, track roadway nearly 70 m range of the bottom of the drum, flake gang, roof cracking, the roadway damage as severe. Therefore, the paper analyzed the spatial overburden structure and stress distribution characteristics of the asymmetric coal pillar area in the mining district, explored the mechanism of coal burst occurrence in the asymmetric isolated coal pillar area, and formulated a coal burst prevention plan for the coal pillar area, aiming to provide a valuable reference for coal burst prevention in the isolated protected coal pillar area under similar conditions.

2. Site Characteristics

2.1. Asymmetric Isolated Coal Pillar Details. For the asymmetric isolated coal pillar in the YaoQiao Coal Mine central mining district, the selected research project was in Xuzhou City, northwest Jiangsu Province, China. Based on preliminary statistics, at least two disastrous coal bursts had previously occurred in this YaoQiao Coal Mine, which has a high coal burst risk and is a characteristic coal mine with coal burst hazards.

The central mining district of YaoQiao Coal Mine is endowed with No. 7 coal seam, having a simple endowment structure. The No. 7 coal seam thickness is 4.59 to 6.19 m (5.47 m on average) with an inclination ranging from 4° to 10° (8° on average); the coal seam has a substantial coal burst impact tendency and a significant mining depth of 650 to 850 m in the central mining district, and the original stress of coal and rock mass is high.

The central mining district adopted double-wing mining, with gradual mining of the working face on both sides of the coal pillar in the main roadway; the district dip protective coal pillar in the mining area had formed an isolated asymmetric structure. The narrowest area of the isolated coal pillar was about 110 m, and the most expansive area was about 180 m. Meanwhile, a fault protection coal pillar of about 90 m in width and 450 m in length was left in the west wing goaf. Figure 1 illustrates the mining district layout.

We first determined the critical layer's bearing level with the thick and hard roofed structure group having different thicknesses and the bearing of the multilayer roof composite structure meeting the relationship in Equation (1) [17]:

$$(q_n)_m = E_m h_m^3 \frac{\sum_{i=m}^{n} \gamma_i h_i}{\sum_{i=m}^{n} \gamma_i h_i^3}, \quad (1)$$

where $(q_n)_m$ is the load of the roof n^{th} on the roof m; m^{th}, n, and i are the roof rock sequence numbers, respectively; E_m and h_m are the elastic modulus and thickness of the m^{th} overburden, respectively; and E_i, h_i, and γ_i are the elastic modulus, thickness, and unit weight of the i^{th} overburden, respectively.

The n^{th} overburden layer satisfies the relationship in Equation (2) for the critical stratum [17]:

$$(q_n)_m < (q_{n-1})_m. \quad (2)$$

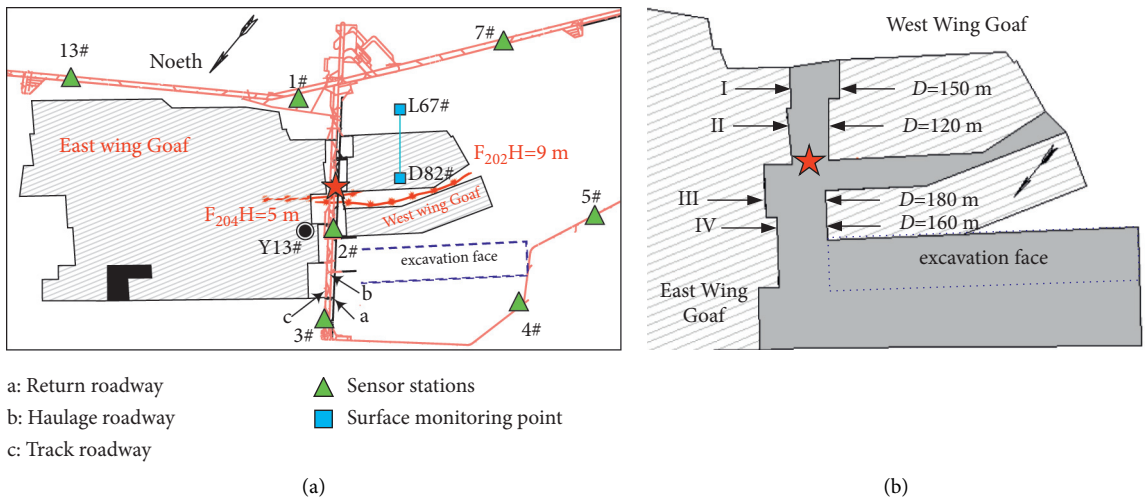

Figure 1: Central mining district district's isolated asymmetric isolated coal pillar arrangement: (a) actual measurement layout; (b) sketch diagram.

The log of central mining district borehole Y13# combined with the roof fracture data observed during the mining period of multiple working faces in the mining district helped determine that the sandstone group 17.0 m away from the coal seam and 26.34 m thick was inferior key strata 1, and the siltstone group 417.0 m away from the coal seam, and 71.34 m thick was the leading fundamental stratum. Meanwhile, the main roof and floor were classed with weak coal burst tendency through laboratory testing for coal burst tendency characterization. Figure 2 gives the critical strata information.

2.2. Analysis of Actual Field Measurement Data. Influenced by the wide range of goaf on both sides of the asymmetric isolated coal pillar, the stress concentration degree of the surrounding rock system in the mining area increased. As a result, the return roadway was affected by high static load stresses, and the shotcrete in most areas of the sides and the upper part of the roadway appeared cracked and hung. Moreover, the bottom drum phenomena occurred in the local area of the roadway floor, as shown in Figure 3.

Microseismic monitoring in mines gave seismic event location and calculation of seismic energy to evaluate the mining stress state and coal burst hazard [18]. A microseismic monitoring system called SOS, developed by the Central Mining Institute of Poland, was installed in the YaoQiao Coal Mine. The maximum locating errors were 20 m in the horizontal direction and 30 m in the vertical direction. The seismic monitoring network from July to October 2018 is shown in Figure 1.

The microseismic activity in the isolated coal pillar area was frequent due to design working face roadway excavation, which indicated that the coal and rock system in the coal pillar area was disturbed by mining, which intensified its stress evolution and rupture activity. Figure 4 illustrates the distribution of microseismic events. Figure 4(a) shows that the microseismic event count and microseismic intensity in the west wing goaf of the central mining district were significantly more than those in east wing goaf; especially the microseismic activity was the most intense between the designed working face and the faulted coal pillar, indicating that the stability of the coal and rock layer was worse in this area. Furthermore, Figure 4(b) shows that microseismic events in the east wing goaf occurred mainly in the high rock layer, while those in the west wing goaf occurred primarily in the low rock layer, indicating that the overburden fissures in the east and west wing goaf of the asymmetric isolated coal pillar area were at different heights.

With a precise picture of the roadway response in the coal pillar area and microseismic monitoring, the asymmetric isolated coal pillar in the mining area was affected by the coal seam mining on both sides. Furthermore, the stress concentration of the roadway surrounding the rock system was high, the overlying rock was highly active, and the roof's stability was unsatisfactory. Therefore, to reduce the safety of the roadway group in the isolated coal pillar area during the design working face excavation and later working face retrieval, it was imperative to study the mechanism of coal burst in the asymmetric isolated coal pillar area.

3. Stress Distribution Characteristics of Coal Seams in Asymmetric Isolated Coal Pillar Area

3.1. Analysis of the Spatial Structure of the Overburden Rock in Isolated Coal Pillar Area

3.1.1. Analysis of the Evolution Pattern of Overburden Fracture. The critical stratum theory suggested that the overlying essential strata controlled all rock activity in the overlying rock layer of the quarry either locally or up to the surface [17]. Meanwhile, the maximum surface subsidence value was related to the mining depth H and L. Therefore, when the L/H value was more significant, it indicated a greater mining degree. Therefore, when the size L of the mining area reached or exceeded (1.2~1.4) H, the surface achieved the full mining degree, and the surface subsidence coefficient did not increase any further [19].

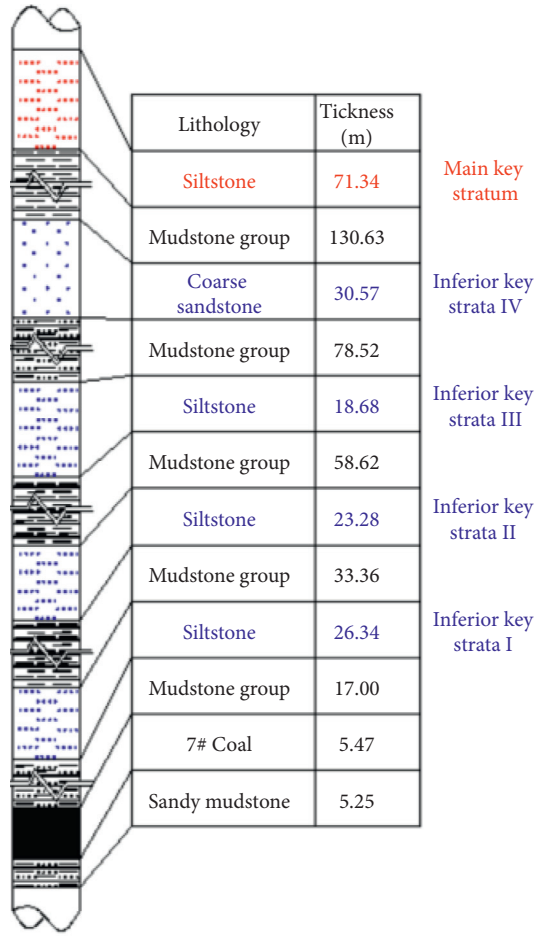

Figure 2: Distribution of main primary and inferior key strata in the asymmetric coal pillar area (borehole Y13#).

(a) (b)

Figure 3: Actual photo of the return roadway: (a) schematic diagram of sidewalls of the roadway sideways and floor heave; (b) schematic diagram of roadway roof cracking.

Based on the current mining status of the working face in the central mining district, the roof collapse of the east wing of the mining area was sufficient for complete extraction. However, the overlying rock fissure development height of the west wing of the mining area was limited, and the roof collapse was not enough, leading to a mining insufficiency (see Table 1).

Meanwhile, the general rock movement theory suggested that the structure's maximum height formed by the fractured rock layer above the quarry during the mining insufficiency phase was one-half of the mined-out area [20]. Then, in the overburden strike profile, the isolated coal pillar I-I section area was an asymmetric "T"-type isolated structure with one entire side, complete extraction, and the

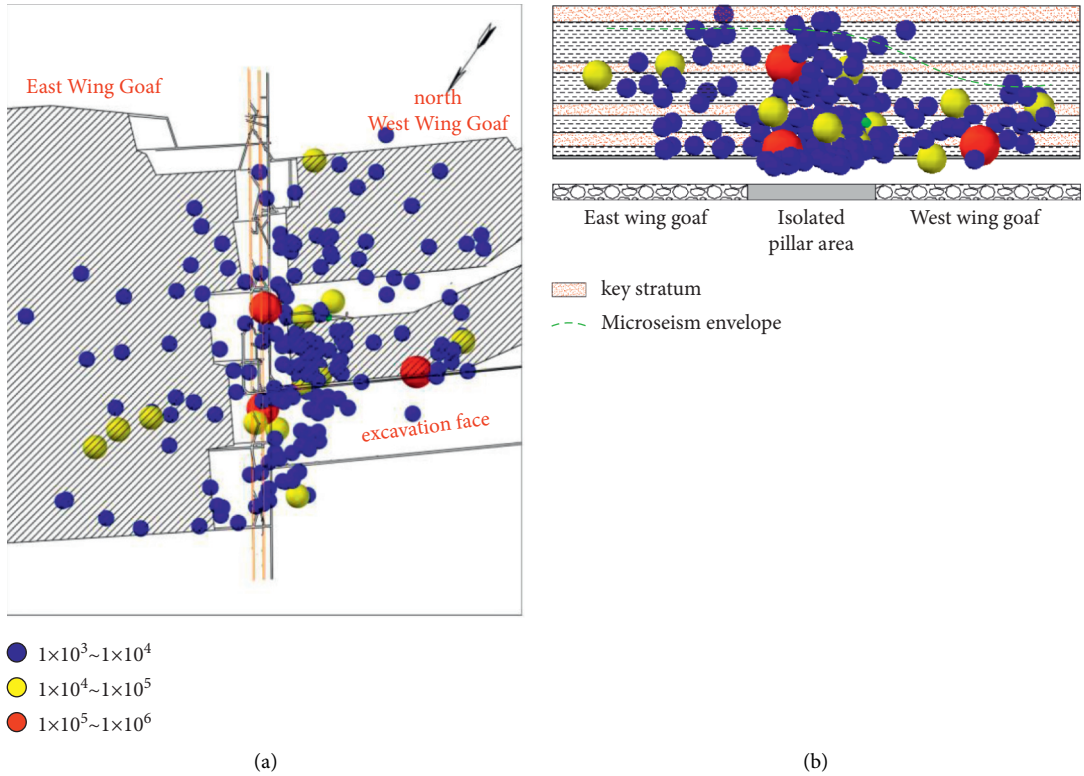

(a) (b)

Figure 4: Microseismic localization map of the asymmetric isolated coal pillar area (2018.01.01~2018.06.30): (a) microseismic positioning plan; (b) microseismic positioning orientation profile.

Table 1: Judgment table for district's mining adoption level.

Position	Goaf length (m)	Goaf width (m)	Mining depth (m)	L/H	Level of adoption
East wing goaf	1610	1100	750	1.47	Full extraction
West wing goaf (I-I section)	650	310		0.41	Insufficiency mining
West wing goaf (III-III section)	700	180		0.24	

other mining insufficiency (the overburden breakage height was about 150 m). Finally, the III-III section area was an asymmetric "T"-shaped isolated structure with one complete side extraction and one side insufficiency mining (the overburden breakage height was about 80 m).

Surface subsidence observation points were established before mining on the west wing of the central mining district, and the measured surface subsidence curves are in Figure 5. According to the surface subsidence monitoring data for October 31, 2018, the surface subsidence from measurement point *L*67 to *D*82 on the surface was 0 to 800 mm using the integral probability method [21].`

$$W_{\max} = qm \cos\beta, \tag{3}$$

where q is the surface submersion coefficient and takes 0.4~0.95; m is the coal seam thickness, $m = 5.47$ m; and β is the dip angle of the coal seam, $\beta = 8^{\circ}$.

Equation (3) yields the empirical range for the maximum ground subsidence on the west wing of the central mining district to be $2{,}160\,\text{mm} < W_{\max} < 5{,}140\,\text{mm}$. Since this ground subsidence on the west wing of the mining area was smaller than the practical minimum subsidence for this area, we inferred that the overlying high essential stratum in the west wing goaf was intact.

Therefore, in the overburden strike profile, the asymmetric isolated coal pillar area in the central mining district was an asymmetric "T"-type isolated coal pillar with one side thoroughly mined and another not fully excavated. In addition, due to the fault-protected coal pillar in the west wing goaf, the overburden breakage height differed on both sides of the fault-protected coal pillar (see Figure 6).

3.1.2. Analysis of Overburden Movement Process. For the asymmetric "T"-type isolated structure in the deep asymmetric isolated coal pillar area, the roof stratum breaking motion process was included [22]: low-stand low key strata tension breaking ⟶ low-stand critical block rotary extrusion ⟶ rotational instability of low-stand low key strata of "T"-type long wall and short wall low-stand typical key strata shear slip instability ⟶ high-stand low key strata tension breaking ⟶ high-stand key block rotary extrusion ⟶ low-stand strata passive instability ⟶ breaking of primary key

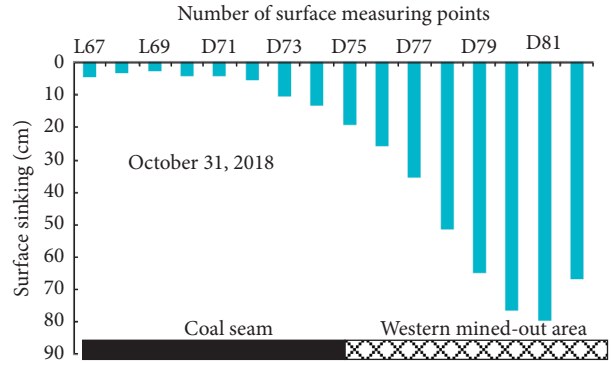

Figure 5: Surface subsidence curve.

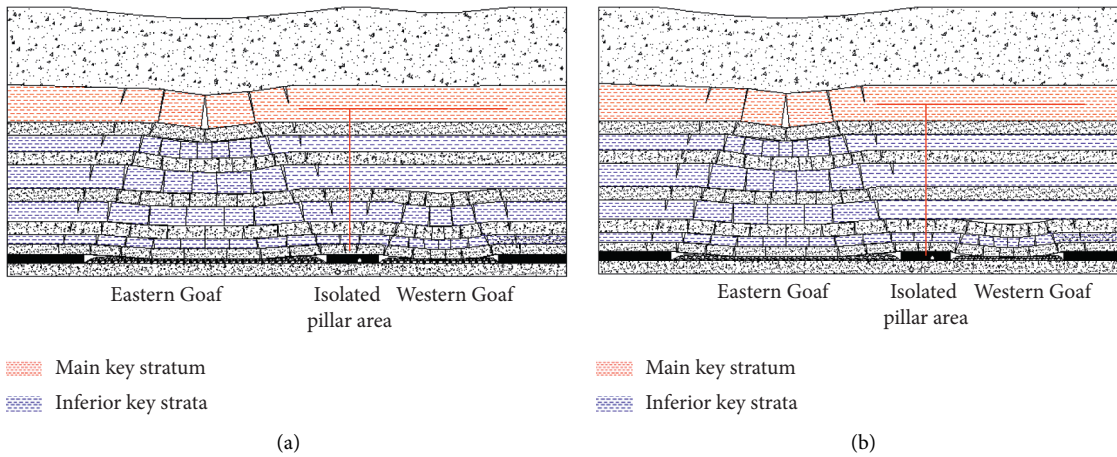

Figure 6: T-type overlying structure of isolated pillar in central mining district: (a) I-I section overburden structure; (b) III-III section overburden structure.

strata of "T"-type long wall. The process of local overburden breaking movement in the isolated coal pillar area is shown schematically in Figure 7.

Therefore, the breaking of critical layers at all levels above the goaf on both sides of the asymmetric isolated coal pillar area, the synergistic movement of overburden rock under significant goaf conditions, and the change of spatial structure will not only cause the increase of stress in the coal and rock layer in the asymmetric isolated coal pillar area. However, also the vibration generated by the breaking of overburden rock will impose a dynamic stress load on the coal and rock layer in the coal pillar area in the form of stress waves, which prompt the destabilization of the surrounding rock system of the roadway in the asymmetric coal pillar area that induced the dynamic coal burst disaster.

3.2. Stress Distribution Characterization in the Isolated Coal Pillar Area. The stress distribution pattern on the isolated coal pillar area in the central mining district varied with width dimension, D of the protected coal pillar, and the influence range S of the oversupporting pressure at the working face. However, there were four different forms [23], as shown in Figure 8.

When the width of the isolated coal pillar was large ($D > 2S$), the coal pillar support capacity was large, and the peak stress was located on both sides of the coal pillar and not superimposed. The central stress of the coal pillar was the original rock stress. At this instance, the supporting pressure distribution on the coal pillar area was a "double-peak" distribution (see Figure 8(a)). When the width of the isolated coal pillar complied with $2S > D > S$, the superimposed support pressure of the working face, the plastic zone of the coal layer on both sides of the hollow mining area gradually extended to the center of the coal pillar. As a result, the stress in the central region of the coal pillar continued to rise and was more significant than the original rock stress but still less than the peak stress. Because the peak support pressure was not yet superimposed, its peak size had not changed. At this instant, the support pressure curve was a "saddle-shaped" distribution (see Figure 8(b)). When the width of the isolated coal pillar was small ($D < S$), the peak support pressure at the edge of the coal column was superimposed. As a result, the uniformly distributed stress value increased in the central region of the coal pillar. The elastic core region was in the external high-stress state for a long time to produce plastic damage. At this time, the support pressure curve was a "platform-shaped" distribution

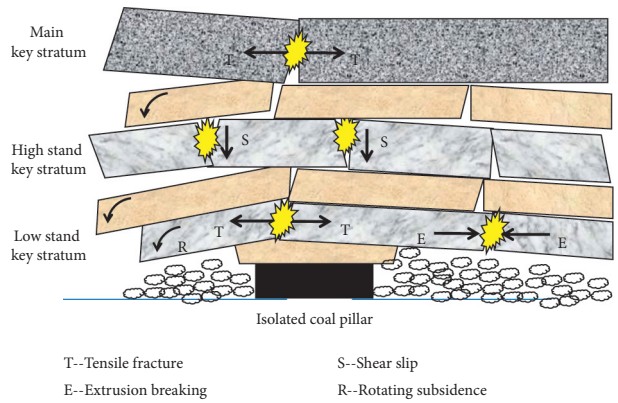

Figure 7: The process of mining earthquake induced by an overburden fracture.

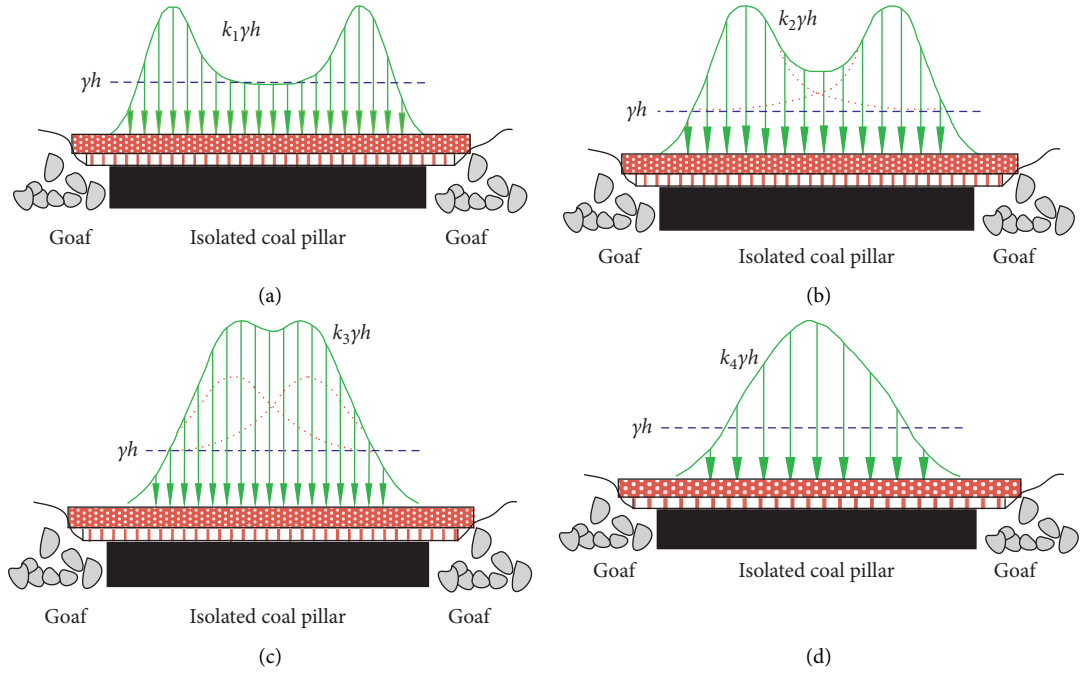

Figure 8: Distribution of superimposed stress field in isolated coal pillar area: (a) double peak; (b) saddle-shaped; (c) platform-shaped; (d) single peak.

(see Figure 8(c)); for a minimum width ($D << S$) of the isolated coal pillar, the plastic zone on both sides of the column was through. The pressure value in the central region of the column is greater than the ultimate strength of the coal seam. At this time, the pillar had no elastic core area, and destabilization was very easy to occur when disturbed by external forces. At this time, the support pressure curve was a "single peak" distribution (see Figure 8(d)).

Based on the historical mining data of the working face in the central mining district, the influence range of the oversupport pressure caused during the active face recovery was generally 80 m. Hence for asymmetrically isolated coal pillars in the central mining district, the width of the pillar was more extensive than 160 m, and the stress of the pillar was characterized by a "double peak" distribution. When the width of the pillar was greater than 80 m and less than 160 m, the stress of the pillar was a "saddle-shaped" distribution; when the width of the pillar was less than 80 m, the stress of the pillar was "platform-shaped" or a "single-peak" distribution. Then, the stress distribution of the coal seam in the asymmetric isolated coal pillar area in the central mining district was initially determined as shown in Figure 9, and the stress pattern in the coal pillar area was mostly a "saddle-shaped" distribution, and the local area was a "double-peak" distribution.

3.3. Distribution Law of Lateral Abutment Pressure in Isolated Coal Pillar Area. The analysis above of stress distribution characteristics in the isolated coal pillar area depended on the relationship between the coal pillar size D and the influence range S of oversupport pressure at the working face. In contrast, the spatial overburden structure in the isolated coal pillar determined the stress transfer mechanism from its

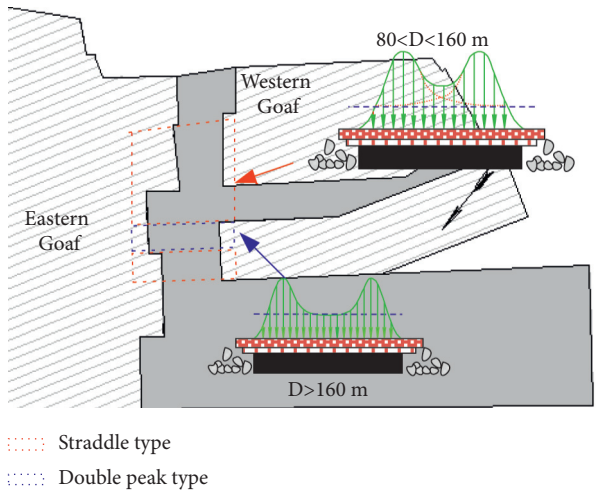

Figure 9: Schematic diagram of stress field distribution characteristics in the isolated coal pillar area.

overburden to the coal layer. Moreover, the different spatial overburden structures directly led to the further stress distribution in the coal pillar.

As shown in Figure 10, the static stress load σ_j in the coal seam around the coal pillar area was mainly composed of the self-weight stress σ_g in the surrounding rock and the stress increments $\Delta\sigma_1$, and $\Delta\sigma_2$ transferred to the isolated coal pillar area from the overlying rock layer in the mining area on both sides [24]. Therefore, the support pressure in the isolated coal pillar area is expressed by the following equation :

$$\sigma_j = \sigma_g + \Delta\sigma_1 + \Delta\sigma_2, \tag{4}$$

where the expression of the self-gravity stress σ_g is as follows:

$$\sigma_g = \gamma H, \tag{5}$$

where γ is the average unit weight of the overlying rock layer, N·m^{-3}, and H is the average depth of the isolated coal pillar, m.

For practical engineering simplicity in calculating the stress transferred from each overburdened critical layer to the coal seam at the working face, its stress is assumed to be an isosceles triangle distribution. Then, the stress increment generated by the i^{th} critical layer was expressed through Equation (6) [24]:

$$\Delta\sigma_{1,2} = \begin{cases} \dfrac{\Delta\sigma_{\max} x \tan\alpha}{H_i}, & \left(0, \dfrac{H_i}{\tan\alpha}\right), \\ \Delta\sigma_{\max}\left(2 - \dfrac{x\tan\alpha}{H_i}\right), & \left(\dfrac{H_i}{\tan\alpha}, \dfrac{2H_i}{\tan\alpha}\right), \\ 0, & \left(\dfrac{2H_i}{\tan\alpha}, +\infty\right), \end{cases} \tag{6}$$

where α is the angle of strata movement (°); H_i is the height of destressed zone, m; and $\Delta\sigma_{\max}$ is the maximum value of the stress increment generated by the overburden of the i^{th} layer of the unilateral mining area on the solitary coal pillar seam,

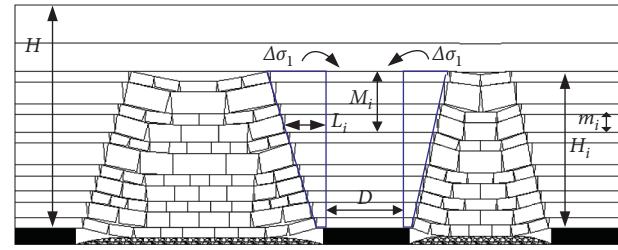

Figure 10: Mechanical model of overlying rock structure.

Pa. The equation for calculating $\Delta\sigma_{\max}$ was derived from the load Q_i transferred to the isolated working face from the fundamental rock block of the i^{th} layer in the adjacent mining area [17].

$$\begin{aligned} Q_i &= \frac{q_i}{2} \\ &= \frac{\gamma L_i (M_i + m_i)}{2}, \end{aligned} \tag{7}$$

where Q_i is the self-weight load of the i^{th} key strata and the overlying rock strata it controls, MPa; L_i is the length of the i^{th} key strata, m; M_i and m_i are the i^{th} key strata thicknesses and the overlying rock layer it controls, m. So then, the stress increment transferred from the overburden layer to the isolated coal pillar mainly depended on the overhanging length of the critical strata, the evolution height of the overburden, and the layer thickness.

Based on the geological data of the asymmetric isolated coal pillar area in the central mining district, the mechanical parameters required to calculate stress distribution in the coal pillar area were as follows in order (see Table 2).

Section II-II's support pressure distribution curve in the isolated coal pillar area was obtained (see Figure 11(a)).

From the support pressure distribution on section II-II, it was evident that the overall asymmetric "saddle-shaped" distribution of coal pillar support pressure was affected by the asymmetric "T"-shaped spatial overburden structure in the isolated coal pillar area. Furthermore, the peak support

Table 2: Overburden parameters for breaking information.

i	H_i (m)	L_i (m)	M_i (m)	m_i (m)	σ_i (MPa)	α (°)	γ (kN·m^{-3})
1	30.15	35.2	26.34	33.36	7.24		
3	88.4	50.8	23.28	58.62	4.89		
2	167.94	65.7	18.68	78.52	3.95	83	25.5
4	271.09	88.6	30.57	130.63	5.47		
5	452.67	134.2	71.34	325	12.21		

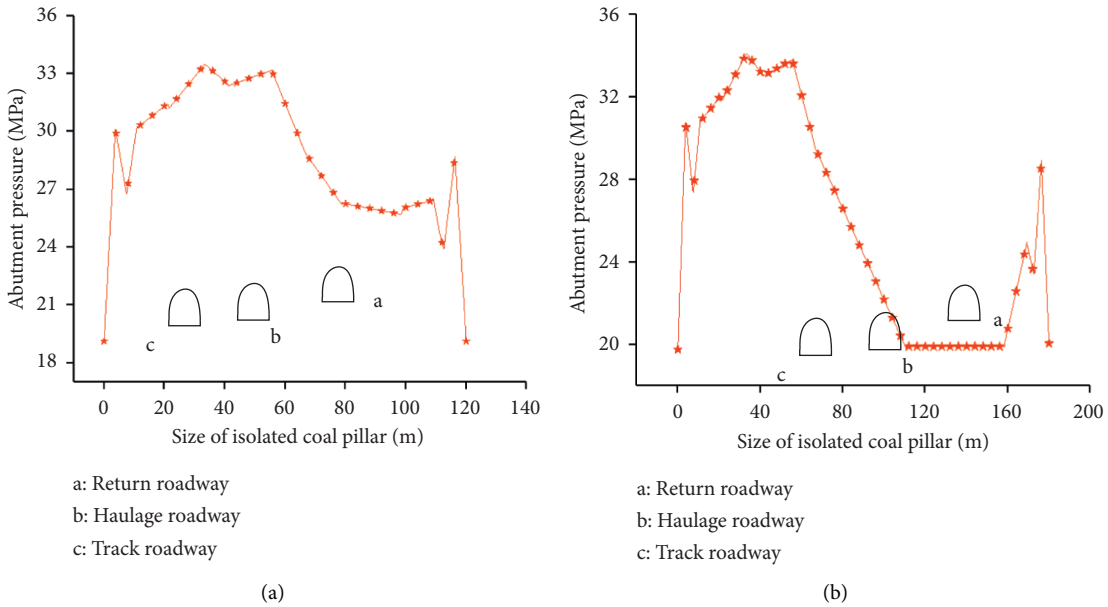

Figure 11: Schematic diagram of supporting pressure distribution in isolated coal pillar area: (a) II-II section; (b) III-III section.

pressure on the east wing goaf was the highest, with a theoretically calculated value of about 33.5 MPa, about 34 m from the edge of the mining area.

Similarly, the overall asymmetric "saddle-shaped" distribution of coal pillar support pressure in the I-I section and IV-IV section, respectively, was theoretically calculated. The overall asymmetric "double-peak" distribution of coal pillar support pressure in the III-III section, with the peak support pressure located on the side of the east wing goaf, is shown in Figure 11(b).

4. Numerical Simulation Analysis of Stress Field in Asymmetric Isolated Coal Pillar Area

4.1. Mining District Modeling. The FLAC3D numerical model was established to study the stress distribution characteristics of the coal and rock layer in the asymmetric isolated coal column area after the recovery of the working face in the central mining district. After simplifying the actual geological conditions in the mining area, the model size was 3,900 × 1,800 × 400 m (X, Y, Z) (see Figure 12). The horizontal and vertical displacement constraints were applied to the bottom at both model ends. As a result, the model's top was a free surface, and a 10 MPa uniform load replaced the overlying rock layer to simulate a 400 m depth. According to the mining practice, the relevant mechanical parameters determined through field geological investigation and relevant parameters obtained from rock mechanics testing were considered in the simulation calculation. The mechanical parameters used in this numerical modeling are in Table 3.

4.2. Characteristics of Static Load Stress Field Distribution in the Isolated Coal Pillar Area. The working faces were excavated following the actual mining sequence in the central mining district. The vertical stress distribution in the isolated coal pillar area is in Figure 13. Affected by the wide range of hollowing in the central mining district and the superposition of oversupport pressure on both sides in the isolated coal pillar area, the overall stress level in the coal and rock layer in the coal pillar area rises, and the stress concentration is high.

Figure 14(a) shows the vertical stress distribution curve of the coal seam under the directional profile of the isolated coal pillar area. It was evident from the figure that the stress distribution in the isolated coal pillar area is an asymmetric "saddle-shaped" distribution. The peak stress was on the side of the east wing goaf due to the different spatial mining scale and overlying rock structure on both sides of the coal pillar area, causing the stress in the eastern part of the coal pillar area to be higher than that in the western region, coupled with the presence of faults in the west wing goaf to protect the coal pillar and play a specific bearing role on the roof. On

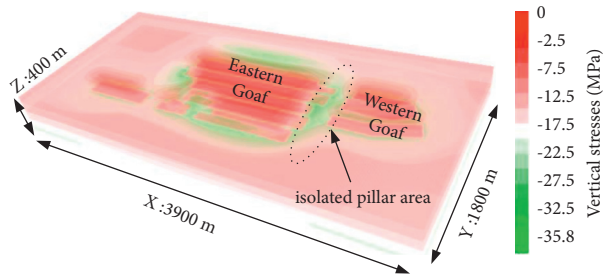

Figure 12: Central mining district model diagram.

Table 3: Main coal and rock mechanics parameters.

Lithology	Density ($kg \cdot m^{-3}$)	Bulk modulus (GPa)	Shear modulus (GPa)	Internal friction angle (°)	Cohesion (MPa)	Tensile strength (MPa)
7#Coal	1 410	1.9	0.9	28	1.2	2.30
Fine sandstone	2 611	11.2	6.0	34	7	10.40
Siltstone	2 589	7.1	3.5	36	8	5.04
Medium-grained sandstone	2 661	10.2	5.0	35	8	8.15
Kern stone	2 636	8.0	4.0	32	9	6.84
Mudstone	2 580	5.8	2.8	33	4	2.83
Sandy mudstone	2 590	6.3	2.9	32	5	3.35

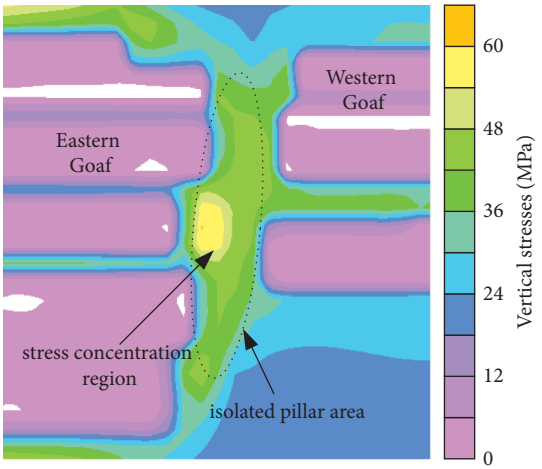

Figure 13: Stress distribution map.

the roadway layout area, the overall stress value of the coal seam showed the trend of track roadway > return roadway > haulage roadway because the return roadway is arranged in the coal seam. The simulation results showed that the stress in the roadway area decreases, but the lateral support pressure affects the site in different ranges in the roadway sides.

Figures 14(b) and 14(c) show the vertical stress and stress increment distribution of the rock layer on the roof of the track and return roadway in the isolated coal pillar area, respectively. The simulation results showed that with the continuous mining of the working face in the mining district, the high-stress area is mainly concentrated in the area of 200~1100 m in the coal pillar area, and the peak stress was at 400~600 m in the coal pillar area, which coincided with the coal burst revealed site in 2016. As a result, the peak vertical stress in the roof of the track roadway increased from 19.25 MPa to 47.6 MPa before mining, with a stress increment of 147%; the peak vertical stress in the return roadway increased from 19.25 MPa to 33.4 MPa before mining. With a stress increment of 73.5%, the peak vertical stress in the isolated coal pillar area continued to increase with the continuous rise of the mining range, the peak stress continued to grow, and the stress concentration coefficient increased. As a result, the stress concentration coefficient increased significantly. At the same time, a second stress peak area appears in the stress distribution in the roof of the track roadway, indicating that the stress shifts to the deeper part of the mining district with the increase of the mining area.

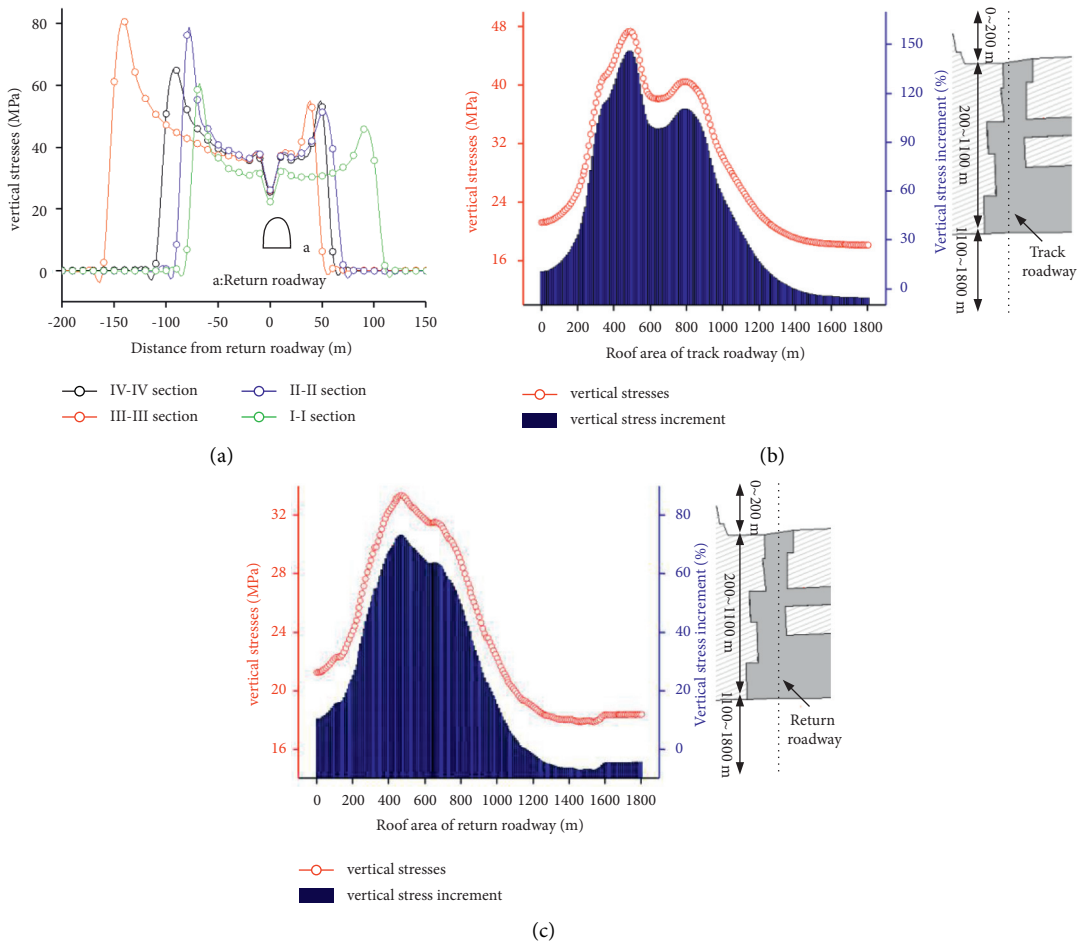

FIGURE 14: Stress change curve of coal and rock mass in isolated coal pillar area: (a) coal seam stress distribution in the coal pillar area (strike profile); (b) stress distribution in track roadway roof (tendency profile); (c) stress distribution in return roadway roof (tendency profile).

The numerical simulation results showed that the stress concentration in the coal and rock layer was high in asymmetric isolated coal pillar areas. As a result, the stress peak in the pillar's middle increased. As a result, the stress shifted to the deep part of the mining district. Furthermore, the stress in the coal seam resulted in an asymmetric "saddle shape." Due to the unreasonable size of the asymmetric isolated coal pillar area, forming a "high stress serrated isolated coal pillar" made the isolated coal pillar area reach the critical state of overall instability impact or unstable failure state.

4.3. Characterization of Dynamic Load Response of Roadway in Isolated Coal Pillar Area. The dynamic load action was applied to the model based on the simulation results for the central mining district under the static load of the asymmetric isolated coal pillar area. Considering that the arranged return roadway was in the coal seam, the monitoring points were set on the roof and floor layers, and the left and right sides of the roadway are seen in the red star area of Figure 1 to monitor the dynamic response characteristics during the dynamic load action. The vibration frequency of the stress wave was 20 Hz, the simulated dynamic load time was two cycles (0.1 s), and the action time was 0.3 s, containing the dynamic load from generation to disappearance. The model mechanical damping was selected as local damping with a coefficient of 0.1571 and set the static boundary.

According to the structural distribution characteristics of study results of the overburden rock in isolated coal pillar, the location of the earthquake source was set in the overburden rock layer of the west wing of the coal pillar III-III section, and the vertical distance of the earthquake source was about 90 m from the coal seam. Therefore, the horizontal distance from the return roadway was almost 100 m. A dynamic load simulation scheme with a specific location for the earthquake source, a 50 MPa dynamic load, was applied to the balanced static load model to monitor the surrounding rock's maximum principal stress evolution characteristics in the return roadway [25].

Figure 15 shows the evolution of the maximum principal stress in the roadway under the condition of 50 MPa dynamic load. Overall, the maximum principal stress at each measurement point characterized that the roadway right side > roadway left side > roadway floor > roadway roof, endorsing that the principal stress is asymmetrically distributed in the rock surrounding the roadway. According to the change rule for the maximum principal stress in the roadway roof, floor, and sides in dynamic load, the curve was

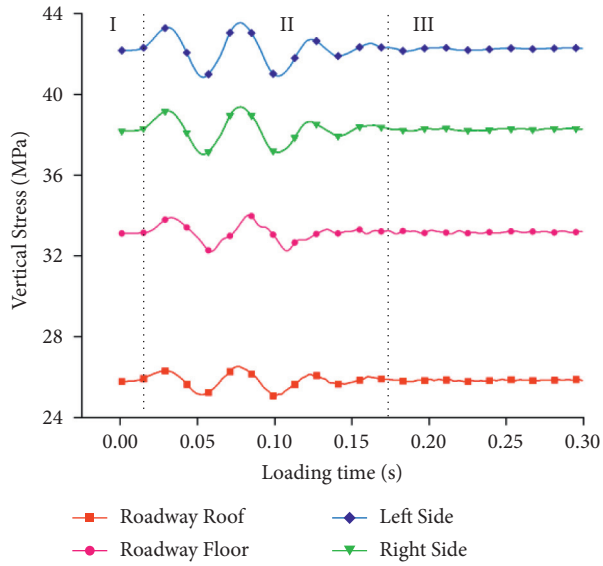

Figure 15: Characteristics of the dynamic load response of the roadway in the isolated coal pillar area.

divisible into three stages. In the first stage (0~0.02 s), the dynamic stress wave had not spread to the monitoring point, and the stress at each monitoring point was the sole result of the static load. Stage II (0.02~0.175 s) process was the active dynamic stage, in that the dynamic stress wave arrived the moment the maximum principal stress in the rock surrounding the roadway began to rise, following the significant decline in the stress wave with cyclic fluctuations and gradual decaying of the vibration amplitude. As a result, under the dynamic load disturbance, the fluctuation amplitude (stress deviation 2.60 MPa) observed on the right side of roadway > roadway left side (stress deviation 2.34 MPa) > roadway floor (stress deviation 1.79 MPa) > roadway roof (stress deviation 1.47 MPa). The characteristics of the maximum principal stress distribution in the surrounding rock conformed to the above observations. In stage III (0.175~0.30 s), the maximum principal stress at each monitoring point was stable, and the stress variation did not exceed 0.1 MPa, indicating that the roadway was not disturbed by the dynamic loading.

The dynamic load simulation results showed that when the coal seam roadway in the isolated coal column area was disturbed by dynamic load under high static load, the stress system in the rock surrounding the roadway produced more significant stress changes, and the roadway was more susceptible to destabilizing damage.

5. Mechanism of Coal Burst Occurrence in Asymmetric Isolated Coal Pillar Area

Coal bursts result from the combination of dynamic stress and static stress. When the dynamic and static stress in the coal and rock mass exceeded the critical stress, the coal burst will be induced [26, 27].

$\sigma_j + \sigma_d \geq \sigma_{Bmin}$, where σ_j and σ_d are static and dynamic stress, respectively, in coal/rock mass induced by microseismic events; σ_{Bmin} is the critical burst stress.

Comprehensive analysis of the coal burst event in the mining district roadway confirmed that the main reason was a high-stress concentration in the coal and rock layers in the area that exceeded the compressive strength of the coal and rock mass. As a result, the local coal burst phenomenon occurred in the roadway. For the asymmetric isolated coal pillar area in the central mining district, the coal pillar formed a "high stress asymmetric isolated coal pillar." Under the action of self-weight stress at significant mining depth and lateral support pressure of the coal pillar, the isolated coal pillar progressively reached the critical state for the overall instability of the coal pillar. Then, under the action of high static load, or when it was disturbed by dynamic load (overburden movement, mining activities, *etc.*), it finally broke through the limiting equilibrium condition for the overall instability impact on the coal pillar area, and the coal burst accident occurred (see Figure 16).

Summarizing the above mechanism of coal burst occurrence of asymmetric isolated coal pillar, the main influencing factors that induced the overall destabilizing impact in the deep asymmetric isolated coal pillar area were: mining depth, the width of protective coal pillar, and overburden space structure. Therefore, the mining depth belonged to the influence factor of geological conditions, and the retention of defensive coal pillar width and overburden space structure belonged to the influence factor of mining technology. The root cause for this kind of coal burst accident was the unsatisfactory size of asymmetric isolated coal pillar, which led to the formation of "high stress serrated isolated coal pillar." The action self-weight stress and lateral supporting pressure from the coal pillar were further affected by other stress superposition, or the concentrated stress of the coal pillar

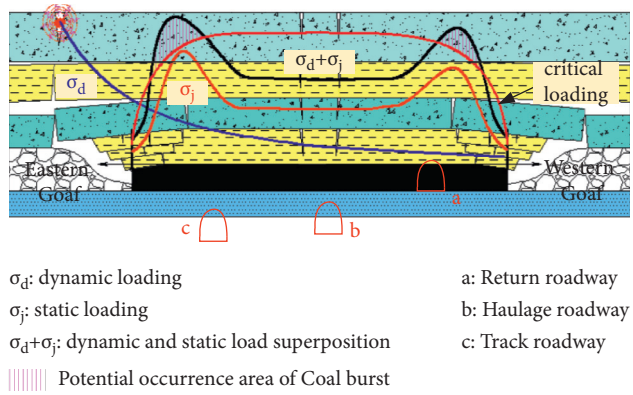

Figure 16: Dynamic and static load superimposed coal burst mechanism in the asymmetric isolated coal pillar area.

exceeded the bearing capacity of the coal seam that facilitated the coal burst phenomenon in the roadway.

6. Coal Burst Prevention and Control Practice in Asymmetric Isolated Coal Pillar Area

6.1. Prevention and Treatment Programs. Based on the above analysis for the mechanism of coal burst in the deep asymmetric isolated coal pillar area, the overall instability of the isolated coal pillar was mainly related to the degree of stress concentration in the coal seam and the spatial structure of the coal seam (the overburden). Therefore, the key to preventing and controlling this type of coal burst was to reduce the concentration of coal seam support pressure in the isolated coal pillar area and reduce the dynamic load disturbance brought by the overburden breakage. In addition, strengthening the roadway support in the coal pillar area effectively prevented and controlled the coal bursts.

To minimize the dynamic load generated from the roof breakage in the isolated coal pillar area caused strong disturbance to the roadway and simultaneously destroyed the integrity of the rock layer, weakened the roof structure, and reduced the length of the overhanging roof, the roof deep-hole precracking blasting cut off actively the overhanging roof and induced the early release of the elastic energy accumulated in the roof. They took the I-I further arranged III-III sections in the isolated coal pillar area as examples. As a result, several roof-deep blasting holes were arranged every 10 m in the mining district roadway [28]. Furthermore, to destroy the integrity of the coal seam in the isolated coal pillar area and reduce the degree of stress concentration in the coal seam, extensive diameter pressure relief drilling of the coal seam is adopted to weaken the coal seam and reduce the stress level of the coal seam in the coal pillar area. The above analysis of the peak stress in the coal pillar area located on the side of the east wing goaf and the track and haulage roadway was in the stress concentration area [29]. Therefore, the deep-hole arrangement was adopted on the left side of the return roadway (corresponding to the eastern part of the coal pillar). Moreover, the usual hole arrangement was adopted on the right side to reduce the stress level in the deep stress peak area of the coal pillar area, with a drill hole arrangement spacing of 2 m. The pressure relief hole arrangement is given in Figure 17, and the pressure relief parameters are in Tables 4 and 5.

6.2. Prevention and Treatment Effect Test

6.2.1. Comparison of Microseismic Monitoring Data. The asymmetric isolated coal pillar area was subjected to multiple rounds of deep-hole blasting off the roof and pressure relief measures of coal seam drilling in the III-III section area from August 1 to August 20, 2018. The microseismic data from July 10 to July 29, 2018 (before unloading pressure) and August 1 to August 20, 2018 (after unloading) were selected for analysis, as shown in Figure 18. After unloading pressure of the isolated coal pillar area, the daily average microseismic release energy decreased from 2.48×10^4 J before unloading to 1.48×10^4 J after unloading, with a reduction of about 40.3%; the daily average microseismic event count decreased from 45 times before unloading to 35 times, with a decrease of approximately 22.2%.

The isolated coal pillar area was subjected to multiple rounds of deep-hole blasting off the roof and pressure relief measures for coal seam drilling in the I-I section area from September 24 to September 29, 2018. Therefore, the microseismic data from September 5 to September 24, 2018 (before unloading pressure) and September 30 to October 18, 2018 (after unloading) were selected for analysis, as shown in Figure 19. After unloading pressure in the isolated coal pillar area, the average daily microseismic release energy decreased from 2.98×10^4 J before decompression to 1.86×10^4 J after decompression, with a reduction of about 37.6%; the average daily microseismic event count decreased from 53 times before decompression to 40 times, with a decrease of approximately 24.5%.

The average daily frequency of microseismic events significantly reduced before and after unloading pressure on the central mining district's asymmetric isolated coal pillar area from the average daily energy release. This reduction was more significant than 20%, indicating the stress level reduced effectively in the rock system surrounding the roadway near the isolated coal pillar area after the decompression.

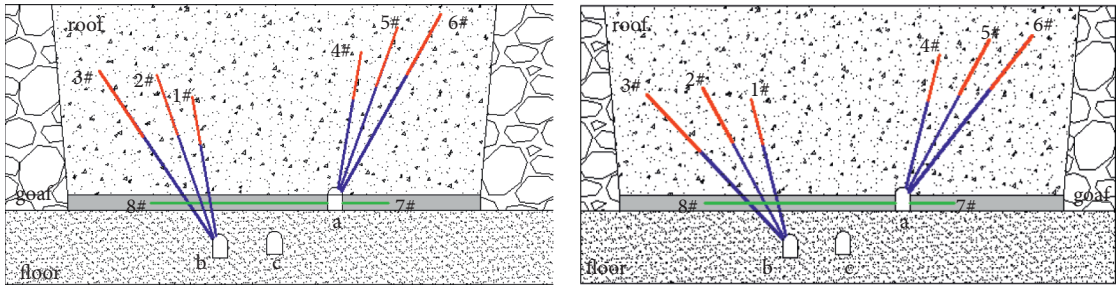

Figure 17: Schematic diagram of pressure relief measures: (a) I-I sections; (b) III-III sections.

Table 4: Parameters of pressure relief measures for I-I section.

Drilling number	Drilling depth (m)	Explosive quantity (kg)	Elevation angle (°)	Loaded length (m)	Hole sealing length (m)	Drilling diameter (mm)
1#	40	48	80	12	16	63
2#	50	60	70	15	20	63
3#	60	80	55	20	22	63
4#	40	50	80	12	16	63
5#	50	60	70	15	20	63
6#	60	80	55	20	22	63
7#	55	—	2	—	—	153
8#	20	—	2	—	—	153

Table 5: Parameters of pressure relief measures for III-III section.

Drilling number	Drilling depth (m)	Explosive quantity (kg)	Elevation angle (°)	Loaded length (m)	Hole sealing length (m)	Drilling diameter (mm)
1#	45	60	75	15	16	63
2#	55	80	60	20	20	63
3#	65	100	45	25	22	63
4#	44	60	75	15	16	63
5#	55	80	60	20	20	63
6#	65	88	50	22	22	63
7#	60	—	2	—	—	153
8#	20	—	2	—	—	153

6.2.2. Analysis of Seismic Computerized Tomography Results. The computerized seismic tomography (seismic CT) inversion evaluation index made a dynamic evaluation of the impact hazard on the working face. The higher the P-wave velocity (V_P) of the coal rock layer of the working face, the larger the positive anomaly coefficient A_n of the wave velocity, indicating that the higher the stress level of the surrounding rock in the area, the more substantial the risk of coal burst [4, 30, 31].

In asymmetric isolated coal pillar areas, coal burst risk was dominated primarily by static stress. Accordingly, Tables 6 and 7 are an assessment criterion compiled for coal burst risk. Velocity anomaly A_n was determined by

$$A_n = \frac{V_p - V_p^a}{V_p^a}, \tag{8}$$

where V_p is the P-wave velocity in a particular medium and V_p^a is the average velocity in the model. It was noteworthy that the zones with positive anomaly and negative anomaly were overstressed and pressure-relieved, respectively.

In the paper, microseismic waveforms in isolated coal pillar area from July 10 to July 29, 2018 (III-III sections before pressure relief) and from August 1 to August 20, 2018 (III-III sections after pressure relief); September 5 to September 24, 2018 (I-I sections before pressure relief); and from September 30 to October 18, 2018 (I-I sections after pressure relief) were selected as seismic computerized

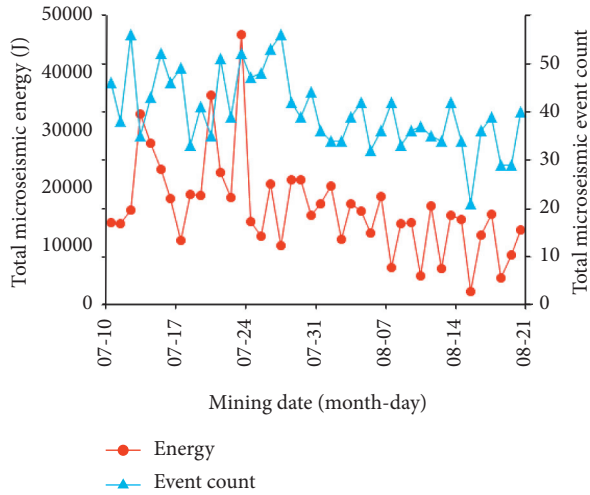

Figure 18: Microseismic monitoring data analysis chart (III-III section).

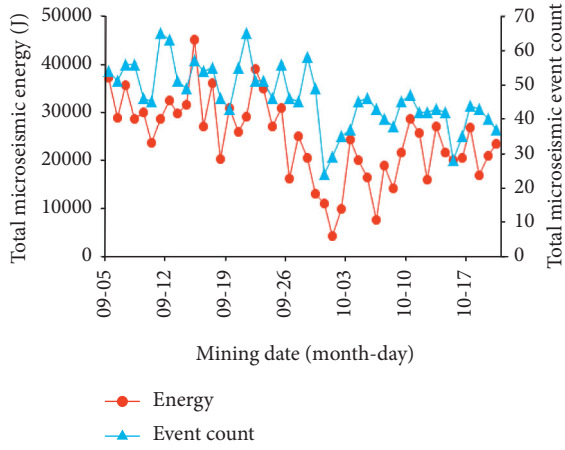

Figure 19: Microseismic monitoring data analysis chart (I-I section).

Table 6: Relation between positive velocity anomalies and coal burst risk level.

Coal burst risk index	Coal burst risk level	Positive velocity anomaly, A_n (%)
0	None	<5
1	Weak	5~15
2	Middle	15~25
3	Strong	>25

Table 7: Relation between negative velocity anomalies and coal burst risk level.

Weakened degree	Weakening characteristics	Negative velocity anomaly, A_n (%)	Stress reduction degree
0	None	0~−7.5	<0.25
−1	Weak	−7.5~−15	0.25~0.55
−2	Middle	−15~−25	0.55~0.8
−3	Strong	<−25	>0.8

tomography data. Furthermore, wave velocity (VP) and the positive anomaly coefficient of wave velocity (An) were used as indicators to evaluate the coal burst risk at the coal pillar area. Figures 20 and 21 show the results of the seismic CT.

The results of the seismic CT in Figure 20 show that the high-stress area before pressure relief was distributed mainly in the area of III-III section in the isolated coal pillar area, with a peak wave velocity of about 6.01 km/s and a peak wave

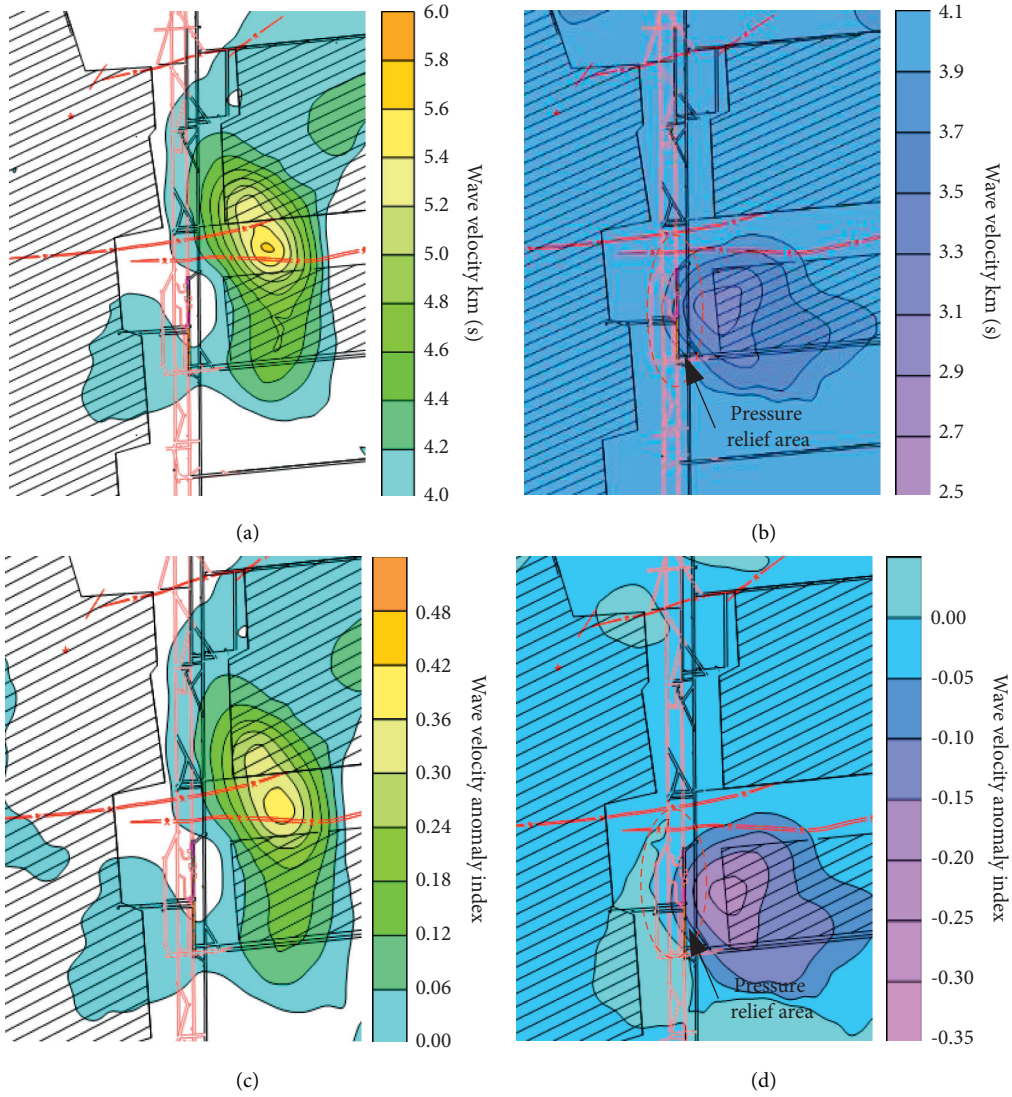

Figure 20: Seismic CT detection results before and after decompression in the III-III section area of the isolated coal pillar. (a) Characteristics of wave velocity distribution before decompression (2018.07.10–2018.07.29). (b)Characteristics of wave velocity distribution after deconfliction (2018.08.01–2018.08.20). (c) Distribution characteristics of wave speed anomaly index (A_n) before decompression. (d) Distribution characteristics of wave speed anomaly index (A_n) after decompression.

velocity positive anomaly index (A_n) of about 0.39. The coal pillar area had a high degree of stress concentration in the rock system's roadway, which impacted coal bursts. The results showed that the peak value of wave velocity was about 3.3 km/s in the isolated coal pillar area after roof deep-hole blasting and coal seam drilling pressure were relieved. After pressure relief, the peak value of wave velocity decreased by 45.1%, and the peak value of the negative anomaly index of wave velocity was about −0.35. Thus, the roof weakened enormously, and the stress concentration in the pressure relief area decreased. The results showed that the stress concentration degree of the rock system surrounding the roadway in Section III-III of isolated coal pillar reduced after pressure relief, and the pressure relief effect was good.

The results of the seismic CT in Figure 21 showed that the high-stress area before pressure relief was distributed mainly in the area of the I-I section in the isolated coal pillar area, with a peak wave velocity of about 5.5 km/s and a peak wave velocity positive anomaly index (A_n) of about 0.38. The coal pillar area had a high-stress concentration in the rock system's roadway, intensely impacting coal bursts. The results showed that the peak value of wave velocity was about 4.0 km/s in the isolated coal pillar area after roof deep-hole blasting and coal seam drilling pressure were relieved. After pressure relief, the peak value of wave velocity decreased by 27.3%, and the peak value of the negative anomaly index of wave velocity was about −0.17. Thus, the roof weakened enormously, and the stress concentration in the pressure relief area decreased. The results showed that the stress concentration degree of surrounding rock system of roadway in Section III-III of isolated coal pillar area reduced after pressure relief, and the pressure relief effect was good.

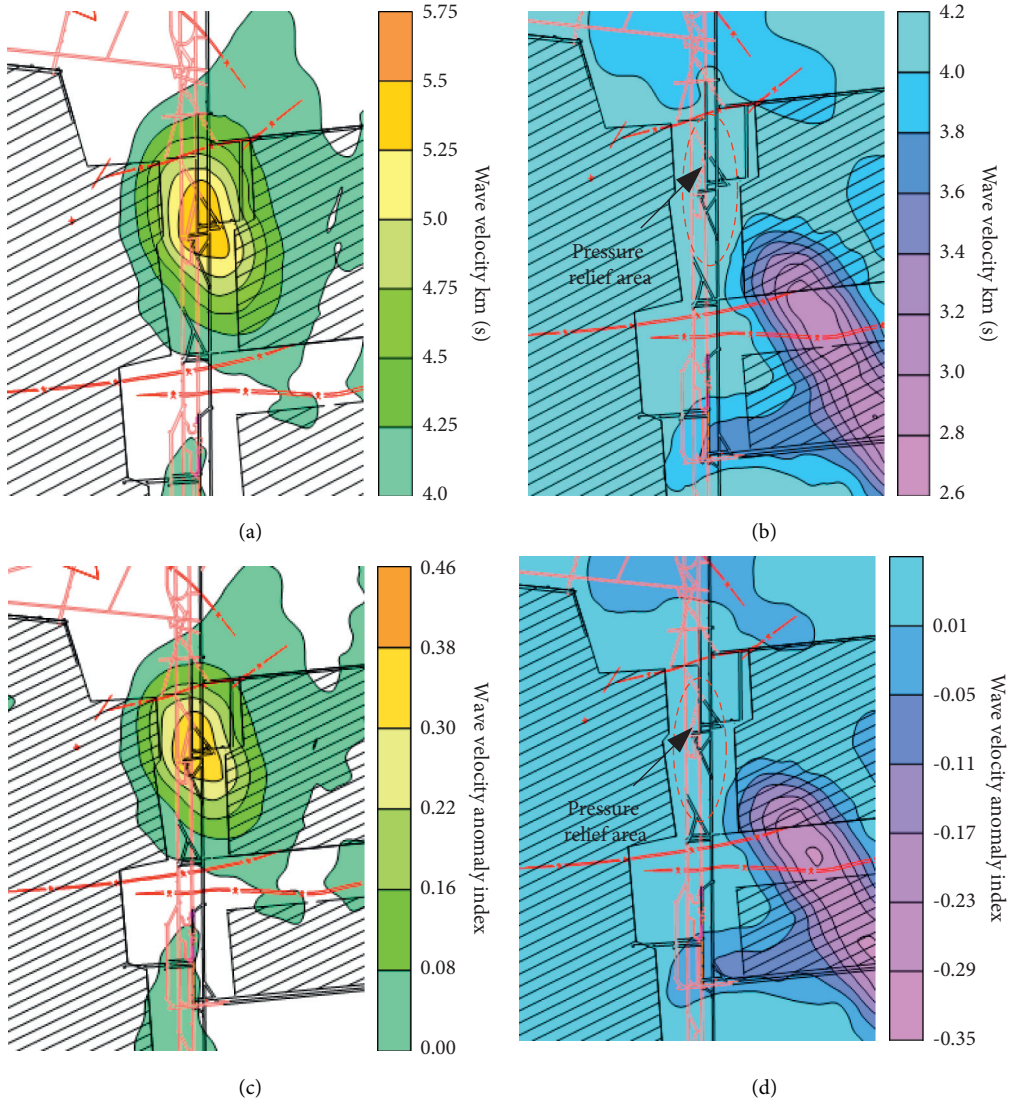

Figure 21: Seismic CT detection results before and after decompression in the I-I section area of the isolated coal pillar. (a) Characteristics of wave velocity distribution before decompression (2018.09.05–2018.09.24). (b) Characteristics of wave velocity distribution after decon-fliction (2018.09.30–2018.10.18). (c) Distribution characteristics of wave speed anomaly index (A_n) before decompression. (d) Distribution characteristics of wave speed anomaly index (A_n) after decompression.

7. Conclusion

(1) Based on the analysis of the overburden structure in the mining district, combined with the surface subsidence data, the asymmetric isolated coal pillar was an asymmetric "T"-shaped isolated structure in the strike-profile, and the overburden breaking movement and spatial structure change on the long wall side of the "T"-shaped led to the stress change of the rock system surrounding the coal pillar area.

(2) The analyzed results of stress distribution in the coal pillar area showed that the stress in the coal seam within the asymmetric isolated coal pillar area was mainly asymmetrical "saddle-shaped" distribution, with local "double peak" distribution, and the peak of the supporting pressure was located in the east wing goaf.

(3) The numerical simulation showed that the stress value on the striking profile of the coal pillar area gradually increased with the increase of the mining area and demonstrated an asymmetric "saddle-shaped" distribution. Furthermore, the peak stress on the tendency gradually increased and gradually shifted to the mining district's deep level, and the peak stress was in the area of 400~600 m of the isolated coal pillar.

(4) The deep asymmetric isolated coal pillar area formed a "high stress asymmetric isolated coal pillar" under the action of factors such as self-weight stress of significant mining depth and lateral support pressure of coal pillar. As a result, the coal pillar was in critical instability under the action of high static load. When disturbed by dynamic load, it was easy to cause the

stress system of the roadway surrounding rock in the coal pillar area to exceed the critical stress for coal burst, thus inducing coal burst accidents.

(5) The deep-hole blasting with a drilled pressure relief scheme in the coal seam was developed for the roof of the coal pillar area to minimize the mechanism of coal bursts induced based on the dynamic and static load on asymmetric isolated coal pillars. The field practice results showed that the pressure relief effect was beneficial; the prevention and control system of asymmetric isolated coal pillar areas in mining districts had a guiding significance for preventing and controlling coal bursts in mines under such conditions.

Data Availability

The data that support the findings of this study are available from the corresponding author upon reasonable request.

Conflicts of Interest

The authors declare that there are no conflicts of interest.

Acknowledgments

The authors gratefully acknowledge the financial support for this work provided by the National Natural Science Foundation of China (Grant nos. 51734009 and 51674253), Postgraduate Research and Practice Innovation Program of Jiangsu Province (Grant no. KYCX21_2380), and Major Scientific and Technological Innovation Projects in Shandong Province (Grant no. 2019SDZY02).

References

[1] L. Dou, T. Chen, S. Gong, H. He, and S. Zhang, "Rockburst hazard determination by using computed tomography technology in deep workface," *Safety Science*, vol. 50, no. 4, pp. 736–740, 2012.

[2] S. J. Gibowicz, *An Introduction to Mining Seismology*, International Geophysics, Warsaw, Poland, 1994.

[3] G. Wang, S. Gong, L. Dou, W. Cai, X. Yuan, and C. Fan, "Rockburst mechanism and control in coal seam with both syncline and hard strata," *Safety Science*, vol. 115, pp. 320–328, 2019.

[4] A. Cao, L. Dou, W. Cai, S. Gong, S. Liu, and G. Jing, "Case study of seismic hazard assessment in underground coal mining using passive tomography," *International Journal of Rock Mechanics and Mining Sciences*, vol. 78, pp. 1–9, 2015.

[5] L. M. Dou, X. Q. He, H. He, J. He, and J. Fan, "Spatial structure evolution of overlying strata and inducing mechanism of rockburst in coal mine," *Transactions of Nonferrous Metals Society of China*, vol. 24, no. 4, pp. 1255–1261, 2014.

[6] H. He, L. Dou, A. Cao, and J. Fan, "Mechanisms of mining Seismicity under large scale Exploitation with Multikey strata," *Shock and Vibration*, vol. 2015, no. 2, 9 pages, Article ID 313069, 2015.

[7] X. Li, Z. Li, E. Wang et al., "Microseismic signal Spectra, energy characteristics, and fractal Features prior to rock burst: a case study from the Qianqiu coal mine, China," *Journal of Earthquake Engineering*, vol. 21, pp. 1–21, 2016.

[8] S. Zhu, F. Jiang, and J. Liu, "Types, occurrence mechanism and prevention of overall instability induced rockburst in China coal mines," *Journal of China Coal Society*, vol. 45, no. 11, pp. 3667–3677, 2020, (in Chinese).

[9] Y. Chen, D. Li, F. Jiang, L. Zhang, C. Wang, and S. Zhu, "Use of the equivalent mining height method for Understanding overlying strata movement and stress distribution in an isolated coal pillar," *Shock and Vibration*, vol. 2020, Article ID 8820886, 12 pages, 2020.

[10] C. Jia, H. Wang, and X. Sun, "Study on rockburst prevention technology of isolated working face with thick-hard roof," *Geomechanics and Engineering*, vol. 20, no. 5, 2020.

[11] J. Hao, J. Chen, and Y. Shi, "Study on the method of prevention and control of dynamic disasters in isolated island face," in *Proceedings of the ninth China-Russia Symposium "Coal in the 21st Century: Mining, Intelligent Equipment, and Environment Protection*, Qingdao, China, October 2018.

[12] J. Fuxing and C. Gong, "Research on overall coal instability of isolated working face with irregular gobs on both sides," *Chinese Journal of Rock Mechanics and Engineering*, vol. 34, no. Sup 2, pp. 4164–4170, 2015, (in Chinese).

[13] D. Li, J. Zhang, and Y. Sun, "Evaluation of rockburst hazard in deep Coalmines with large protective island coal pillars," *Natural Resources Research*, vol. 30, no. 5, 2020.

[14] G. Zhu, H. Liu, Q. P. Jiang, and H. Y. Liu, "Reasonable determination of Terminal mining Lines using the stress field with seismic wave Excitation in deep Coalfaces," *Shock and Vibration*, vol. 2021, Article ID 3929004, 13 pages, 2021.

[15] G. Reed, K. Mctyer, and R. Frith, "An assessment of coal pillar system stability criteria based on a mechanistic evaluation of the interaction between coal pillars and the overburden," *International Journal of Mining Science and Technology*, vol. 27, no. 1, pp. 9–15, 2017.

[16] M. Hamid, "Coal pillar mechanics of violent failure in U.S. Mines," *International Journal of Mining Science and Technology*, vol. 27, no. 3, pp. 387–392, 2017.

[17] M. Qian, X. Miao, and J. Xu, "Theoretical study of key stratum in ground control," *Journal of China Coal Society*, no. 3, pp. 2–7, 1996, (in Chinese).

[18] A. Y. Cao, L. M. Dou, C. B. Wang, and X. . Gu, "Microseismic Precursory characteristics of rock burst hazard in mining areas near a large Residual coal pillar: a case study from Xuzhuang coal mine, Xuzhou, China," *Rock Mechanics and Rock Engineering*, vol. 49, no. 11, pp. 1–16, 2016.

[19] C. Ma, X. Cheng, and Y. Yang, "Investigation on Mining Subsidence Based on Multi-Temporal InSAR and Time-Series Analysis of the Small Baseline Subset-Case Study of Working Faces 22201-1/2 in Bu'ertai mine, Shandong Coalfield, China," *Remote Sensing*, vol. 8, no. 11, 2016.

[20] F. Jing, Y. Liu, and Y. Zhang, "A three-zone structure loading model of overlying strata and its application on rockburst prevention," *Chinese Journal of Rock Mechanics and Engineering*, vol. 35, no. 12, pp. 2398–2408, 2016, (in Chinese).

[21] Z. F. Yang, Z. W. Li, J. J. Zhu, J. Hu, Y. J. Wang, and G. L. Chen, "InSAR-based model parameter Estimation of probability integral method and its application for Predicting mining-induced horizontal and vertical displacements," *IEEE Transactions on Geoscience and Remote Sensing*, vol. 54, no. 8, pp. 4818–4832, 2016.

[22] J. Wang, J. Ning, and L. Jiang, "Structural characteristics of strata overlying a fully mechanized longwall face: a case study," *Journal of the Southern African Institute of Mining and Metallurgy*, vol. 118, no. 11, pp. 1195–1204, 2018.

[23] H. Zhu, P. Liu, and Z. C. Tong, "Numerical simulation research and application on protected layer pressure relief affection under different coal pillar width - Science Direct," *Procedia Engineering*, vol. 84, pp. 818–825, 2014.

[24] G. A. Zhu, L. M. Dou, A. Y. Cao et al., "Assessment and analysis of strata movement with special reference to rock burst mechanism in island longwall panel," *Journal of Central South University*, vol. 24, no. 12, pp. 2951–2960, 2017.

[25] J. He, "Research of Mining Dynamic Loading Effect and its Induced Rock Burst in Coal Mine," Dissertation, China University of Mining and Technology, Xuzhou, China, 2013.

[26] W. Cai, X. Bai, and G. Si, "A monitoring investigation into rock burst mechanism based on the coupled theory of static and dynamic stresses," *Rock Mechanics and Rock Engineering*, vol. 53, no. 12, pp. 1–21, 2020.

[27] J. He, L. Dou, S. Gong, J. Li, and Z. Ma, "Rock burst assessment and prediction by dynamic and static stress analysis based on micro-seismic monitoring," *International Journal of Rock Mechanics and Mining Sciences*, vol. 93, pp. 46–53, 2017.

[28] W. Zhang, X. Qu, C. Li et al., "Fracture analysis of multi-hard roofs based on microseismic monitoring and control techniques for induced rock burst: a case study," *Arabian Journal of Geosciences*, vol. 12, no. 24, 2019.

[29] C. Wang, A. Cao, G. Zhu, G. Jing, J. Li, and T. Chen, "Mechanism of rock burst induced by fault slip in an island coal panel and hazard assessment using seismic tomography: a case study from Xuzhuang colliery, Xuzhou, China," *Geosciences Journal*, vol. 21, no. 3, pp. 469–481, 2017.

[30] H. Navid, "Evaluation of the rockburst potential in longwall coal mining using passive seismic velocity tomography and image subtraction technique," *Journal of Seismology*, vol. 21, no. 5, pp. 1101–1110, 2017.

[31] G. Zhu, L. Dou, and Z. Ding, "Experimental study on rock burst of coal samples under overstress and triaxial unloading," *Meitan Xuebao/Journal of the China Coal Society*, vol. 43, no. 5, pp. 1258–1271, 2018.